Acta Crystallographica Section D
Biological Crystallography
ISSN 0907-4449

A Rac1–GDP trimer complex binds zinc with tetrahedral and octahedral coordination, displacing magnesium

Gerd Prehna and C. Erec Stebbins*

Laboratory of Structural Microbiology, Rockefeller University, New York, NY 10021, USA

Correspondence e-mail: stebbins@rockefeller.edu

Received 23 February 2007
Accepted 8 March 2007

PDB Reference: Rac1–GDP–Zn complex, 2p2l, r2p2lsf.

The Rho family of small GTPases represent well characterized signaling molecules that regulate many cellular functions such as actin cytoskeletal arrangement and the cell cycle by acting as molecular switches. A Rac1–GDP–Zn complex has been crystallized in space group $P3_221$ and its crystal structure has been solved at 1.9 Å resolution. These trigonal crystals reveal the unexpected ability of Rac1 to coordinate Zn atoms in a tetrahedral fashion by use of its biologically relevant switch I and switch II regions. Upon coordination of zinc, the switch I region is stabilized in the GDP-bound conformation and contributes to a Rac1 trimer in the asymmetric unit. Zinc coordination causes switch II to adopt a novel conformation with a symmetry-related molecule. Additionally, zinc was found to displace magnesium from its octahedral coordination at switch I, although GDP binding remained stable. This structure represents the first reported Rac1–GDP–Zn complex, which further underscores the conformational flexibility and versatility of the small GTPase switch regions.

1. Introduction

The Rho family of small GTPases consists of a group of well characterized signaling molecules that regulate a variety of cellular functions. This family of genes is a subset of the ubiquitously expressed Ras-related small GTPases and act as the signal regulators of actin cytoskeletal rearrangement, microtubule dynamics, vesicle trafficking, cell-cycle control and cell motility, among other functions (Symons & Settleman, 2000; Jaffe & Hall, 2005). These membrane-localized molecules regulate the aforementioned cellular processes by acting as molecular switches, cycling between an 'off' and 'on' state in response to extracelluar stimuli such as cytokines, cell-adhesion molecules and bacterial invasion (Symons & Settleman, 2000; Aktories & Barbieri, 2005).

Rho-GTPases localize to the cell membrane owing to an isoprenyl modification at a C-terminal cysteine residue and achieve an 'off' and 'on' biological state by cycling between GDP (guanosine-5′-diphosphate) and GTP (guanosine-5′-triphosphate) bound forms. The Rho-GTPase GDP/GTP cycle is controlled in the cell by three known families of regulatory molecules: GEFs, GAPs and GDIs. GEFs (guanine nucleotide-exchange factors) promote the exchange of GTP for GDP, thus catalyzing activation and turning the system 'on', whereas GAPs (GTPase-activating proteins) stimulate the intrinsic rate of GTP hydrolysis in the Rho-GTPases, turning the system 'off'. Finally, RhoGDIs act as a master control switch for the system, removing the small GTPase from the membrane and inhibiting nucleotide dissociation (Van Aelst & D'Souza-Schorey, 1997; Jaffe & Hall, 2005).

At the molecular level, these signaling events are achieved through conformational changes in the Rho-GTPases at the so-called 'switch' regions. Switch I (residues 29–40, Rac1 numbering) and switch II (residues 55–74, Rac1 numbering) adopt discrete canonical conformations based on the presence of GDP or GTP (Hirshberg *et al.*, 1997; Wei *et al.*, 1997). In the GTP-bound form, the Rho-GTPases are recognized by downstream effectors, many of which are kinases, which are activated owing to a conformational change upon Rho-GTPase binding, releasing a functional domain from an inactivation domain (Maesaki *et al.*, 1999; Bishop & Hall, 2000). The cellular regulators of the small GTPase signaling cycle (GEFs, GAPs and GDIs) also modulate the Rho-GTPases by interacting with the switch regions, adjusting the conformations of the switch regions to promote the relevant biochemistry of nucleotide exchange, GTP hydrolysis and inhibition of nucleotide dissociation, respectively (Vetter & Wittinghofer, 2001; Hakoshima *et al.*, 2003; Dvorsky & Ahmadian, 2004).

As the Rho-GTPases are the control switches for many important cellular processes (Jaffe & Hall, 2005) and are the targets of several bacterial pathogens (Aktories & Barbieri, 2005), these signaling molecules have been extensively studied. In fact, much work has been devoted to revealing their molecular structures alone and in complex with their regulators and effectors in order to gain a better understanding of their normal cellular function and how their function is subverted by bacterial virulence factors. To date, the crystal structures of the most extensively characterized Rho-GTPases (RhoA, Rac1 and Cdc42) have been solved in both the GDP- and GTP-bound states and in complex with a variety of eukaryotic effectors and bacterial virulence factors, except for a Rac1–GDP complex without a bound effector (Hakoshima *et al.*, 2003; Dvorsky & Ahmadian, 2004).

Here, we present the crystal structure of a Rac1–GDP–Zn complex at a resolution of 1.9 Å. This complex not only reveals the surprising ability of Rac1 to coordinate zinc with its biologically relevant (switch) regions, but also demonstrates that zinc can play the role of magnesium in the ability of Rac1 to bind GDP. In this complex, the switch I region is stabilized in the GDP-bound conformation, while zinc fills the octahedral coordination role of magnesium with GDP. The switch II region of this Rac1–GDP–Zn complex adopts a novel conformation owing to its involvement in zinc coordination with a symmetry-related Rac1 molecule. These structural data show that zinc can induce conformational changes within the biologically important switch regions, which further underscores the conformational adaptability and ability for modulation of the Rho-GTPase switch regions.

2. Materials and methods

2.1. Purification of Rac1–GDP

Rac1 1–184 (F78S) was cloned as an N-terminal GST fusion in the vector pGEXT4T3 (Stebbins & Galan, 2000). The GST-Rac1 fusion protein was expressed in *Escherichia coli* BL21(DE3) cells by overnight induction with 1 m*M* IPTG at 293 K. Cells were resuspended in lysis buffer (20 m*M* Tris pH 7.5, 200 m*M* NaCl and 1 m*M* DTT) plus 1 m*M* PMSF and were lysed with an Emusiflux-C5 (Avestin). Cell debris was removed by centrifugation and the supernatant was passed over a Q-Sepharose gravity column followed by a glutathione-Sepharose gravity column. The glutathione-Sepharose column was washed with five column volumes of wash buffer (20 m*M* Tris pH 7.5, 500 m*M* NaCl and 2 m*M* DTT) followed by elution of GST-Rac1 in lysis buffer plus 10 m*M* glutathione. GST was removed by overnight cleavage with thrombin during dialysis into lysis buffer plus 2.5 m*M* $CaCl_2$. The digest was then passed by gravity flow over a heparin Sepharose column to remove thrombin, followed by dilution in 20 m*M* Tris pH 7.5, 1 m*M* DTT to lower the salt concentration for ion-exchange chromatography. GST was separated from Rac1 by passing the digest over a Q Sepharose column followed by an SP FF Sepharose column by FPLC (GE Healthcare). Finally, Rac1 1–184 GDP was concentrated to 60 mg ml^{-1} and run through an SD200 gel-filtration column (GE Healthcare) to isolate non-aggregated material and to exchange the buffer to 20 m*M* Tris pH 7.5, 50 m*M* NaCl and 1 m*M* DTT. All purification steps were performed at 277 K.

2.2. Crystallization and data collection

Rac1 was combined with reductively methylated YpkA 434–732 as previously reported and screened for crystallization (Prehna *et al.*, 2006). The complex was concentrated to 39 mg ml^{-1} and Rac1 crystals were found to grow after initial YpkA precipitation at 277 K by hanging-drop vapor diffusion using a 1:1 mixture of protein solution and well solution, which consisted of 100 m*M* MES pH 6.0, 15 m*M* $ZnSO_4$ and 10% PEG MME 550. Rac1 crystals were further optimized by microseeding using a 'seed-bead' from Hampton Research. Diffraction-quality crystals could be grown in pH conditions ranging from 5.5 to 7.5, 5–20% PEG MME 550 and 1–40 m*M* $ZnSO_4$. $ZnSO_4$ was necessary for crystallization and could not

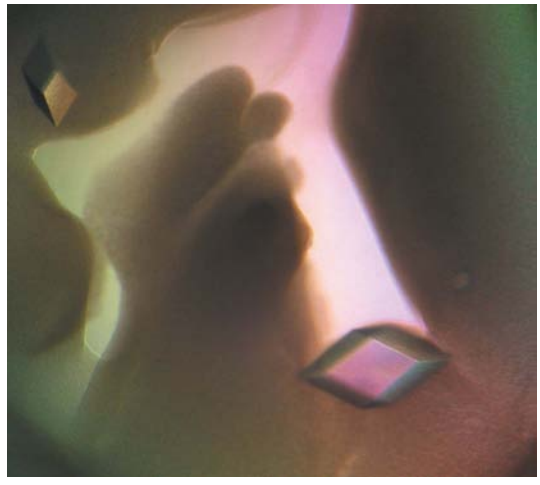

Figure 1
Rac1–GDP–Zn complex crystals. Crystals grown in hanging drops were imaged under plane-polarized light at 100× magnification.

Table 1
Rac1 data-collection and refinement statistics.

Data collection	
Space group	$P3_221$
Unit-cell parameters (Å, °)	$a = b = 89.7$, $c = 191.6$, $\alpha = \beta = 90.0$, $\gamma = 120.0$
Resolution (Å)	77.62–1.90
No. of reflections	548625
No. of unique reflections	70803
R_{sym} or R_{merge}	10.0 (51.2)
$I/\sigma(I)$	18.2 (3.7)
Completeness (%)	99.9 (100.0)
Redundancy	7.7
Refinement	
Resolution (Å)	77.62–1.90
No. of reflections	67009
R_{work}/R_{free}	17.4/20.8
No. of atoms	
All atoms	5129
Protein	4141
Water	896
GDP	84
Zinc	8
B factors (Å^2)	
All atoms	27.6
Protein	33.1
Water	42.6
GDP	20.7
Zinc	31.3
R.m.s. deviations	
Bond lengths (Å)	0.014
Bond angles (°)	1.638

be replaced by $MgSO_4$. Crystals formed in the trigonal space group $P3_221$, with unit-cell parameters $a = b = 89.7$, $c = 191.6$ Å. Data were collected on a MAR CCD 165 detector at beamline X3A at Brookhaven National Laboratory. For data collection, Rac1 crystals were frozen by a stepwise exposure to cryo-buffer (15%, 25% and 28% PEG MME 550 plus mother liquor) and then flash-frozen in liquid nitrogen. The frozen crystals were transferred directly to the cold stream at 93 K. Data were obtained from one crystal to 1.9 Å resolution at a wavelength of 1.284 Å. The data were processed using the *HKL* software package (Otwinowski & Minor, 1997).

2.3. Structure determination and refinement

The phases of the Rac1–GDP structure were determined by molecular replacement using the program *Phaser* as part of the *CCP*4 suite of programs (Collaborative Computational Project, Number 4, 1994; Potterton *et al.*, 2003), using Rac1 (PDB code 1mh1) and YpkA (PDB code 1h7o) as search models. The molecular-replacement solution revealed that only Rac1 was present. The model was initially refined with *REFMAC*5 (Murshudov *et al.*, 1997) from the *CCP*4 suite of programs (Collaborative Computational Project, Number 4, 1994; Winn *et al.*, 2001, 2003; Potterton *et al.*, 2003; Winn, 2003) and then rebuilt using *ARP*/*wARP* (Perrakis *et al.*, 1999). The rebuilt model was further refined with *REFMAC*5 to give final R_{work} and R_{free} values of 17.4% and 20.8%, respectively, with 92.0% of the residues in the most favored regions of the Ramachandran plot and no outliers. Zinc sites were found using the program *SOLVE* (Terwilliger, 2004) and then placed into the molecular-replacement solution. Buried surface areas were calculated using *CNS* (Brünger *et al.*, 1998). All crystallographic figures were generated using the program *PyMOL* (DeLano, 2002).

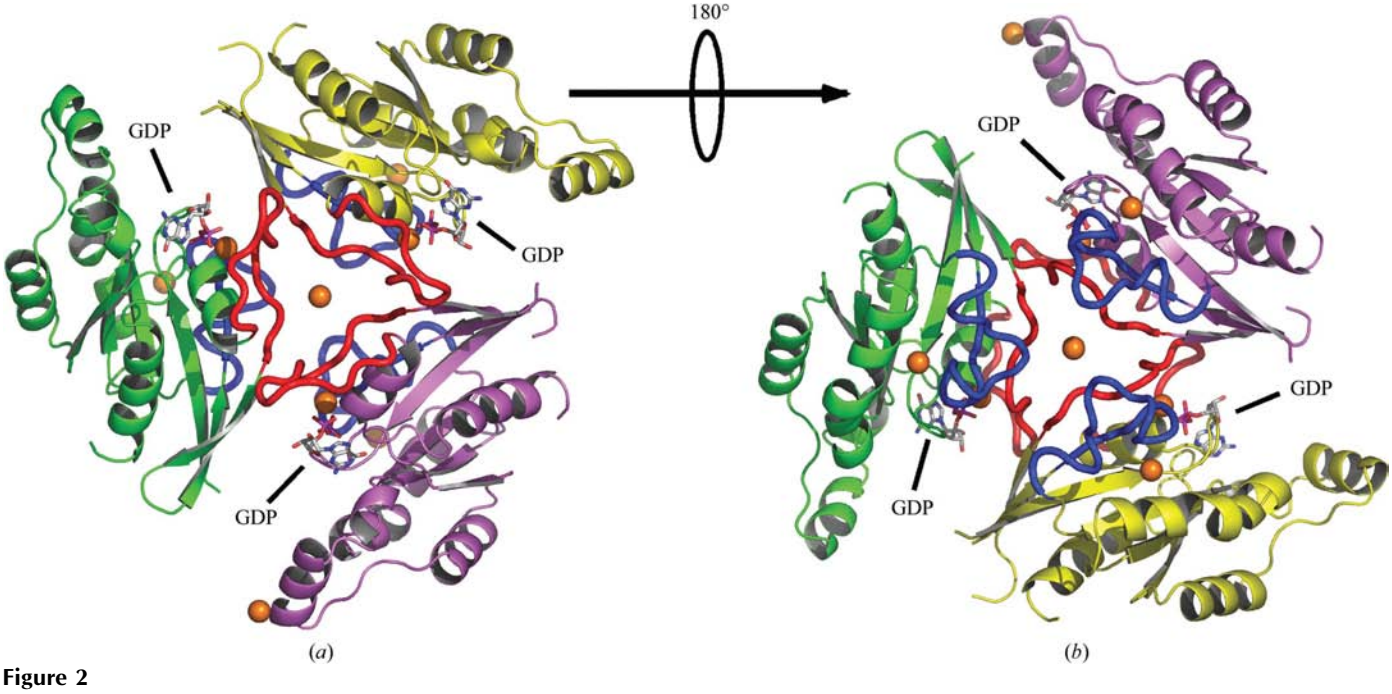

Figure 2
Overall crystal structure of the Rac1–GDP–zinc complex. (*a*) The trimeric Rac1 complex is shown with chain *A* in violet, chain *B* in yellow and chain *C* in green. Switch I is indicated in red, switch II in blue and zinc in dark orange. The three GDP molecules are labeled. (*b*) The trimeric Rac1 complex after a 180° rotation from (*a*).

3. Results and discussion

3.1. Overall structure of Rac1–GDP–Zn complex

Initial crystal screening was performed as described in §2 and produced a condition containing a high concentration of zinc (15 m*M* $ZnSO_4$), which caused intense precipitation followed by subsequent crystal formation (Fig. 1). A data set was obtained on a rotating copper-anode source using a Rigaku IV^{++} detector and was processed to a final resolution of 2.2 Å (data not shown). To generate initial phases, molecular replacement was employed using the program *Phaser* (see §2). The final solution structure contained three Rac1 molecules arranged as a trimer, with an *R* factor and R_{free} of 19.2% and 23.6%, respectively. Based on the crystallization conditions and visual inspection, four zinc-coordination sites were initially found and magnesium was modeled into its predicted site at switch I. To verify the presence of zinc within the crystal, another primary data set was taken at the Zn *K* absorption edge (see §2) and the zinc sites were found by single anomalous dispersion using the program *SOLVE* to analyze the anomalous differences. The initial molecular-replacement solution was refined against the new data set with the experimental zinc sites placed (Table 1).

The Rac1–GDP complex consists of three Rac1 molecules in the asymmetric unit that are related to each other by a threefold noncrystallographic axis of symmetry. Each monomer not only contains the expected GDP, but also contains two zinc ions (Fig. 2). At the center of the noncrystallographic threefold axis there is an additional zinc that is coordinated by residues from switch I (Fig. 3*a*) and a final zinc that links chain *A* and chain *C* from symmetry-related molecules (Figs. 2 and Fig. 3*d*). The Rac1 molecules in the asymmetric unit are almost identical, having low root-mean-square deviations as calculated from the C^{α} trace. The highest r.m.s.d. calculated using the C^{α} trace was between chain *A* and chain *B* and had a value of 0.42 Å. Although the Rac1 monomers are highly identical, there are small differences in areas of high disorder. None of the Rac1 monomers contain density for the N-terminal cloning artifact present in the protein sequence from the GST affinity tag linker (see §2) and all three chains have poor density from residues 45 to 50. In this loop region connecting β-sheets 2 and 3, chain *A* is missing density for residues 45, 46 and 47, and chain *B* is missing density for residue 49. Additionally, both chain *B* and chain *C* have poor side-chain density in an α-helical region from residues 121 to 130 (chain *B*) and residues 121 to 124 (chain *C*). Finally, no density is seen in any of the monomers C-terminal to residue 179.

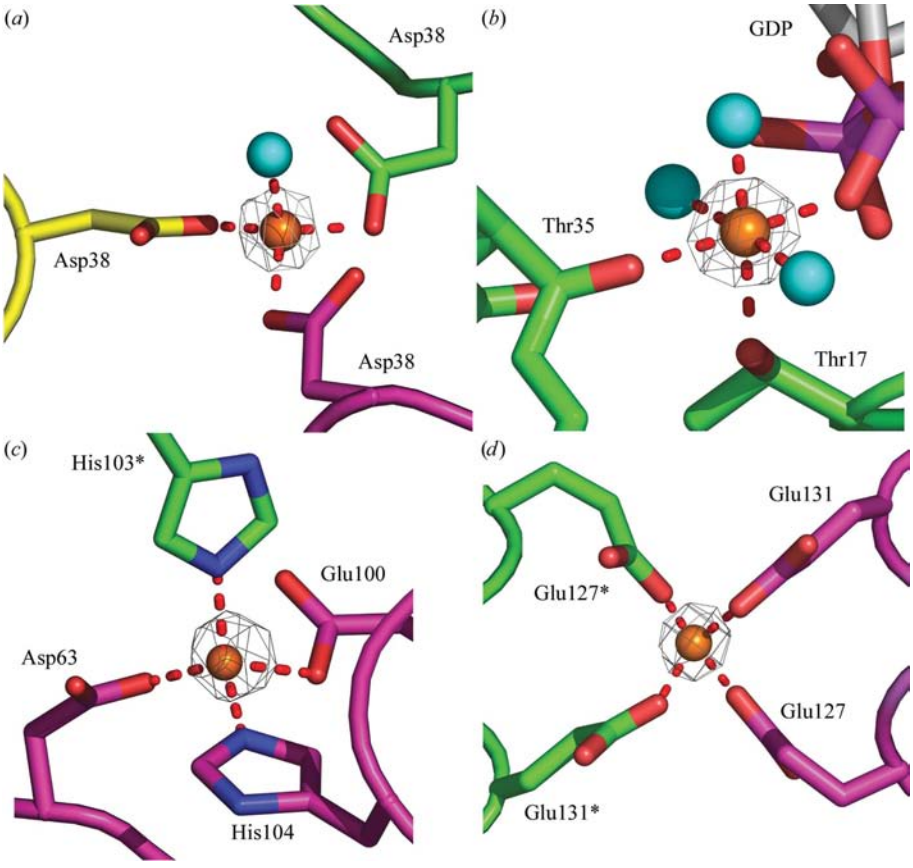

Figure 3
Rac1 zinc-coordination sites. (*a*) The coordination of zinc by switch I. Chain *A* is shown in magenta, chain *B* in yellow and chain *D* in green. Zinc is shown in dark orange and the coordinated water molecule in light blue. The dashed red lines indicate the zinc-coordination interactions. The $F_o - F_c$ map is show in gray at 20σ and was calculated without zinc. (*b*) Zinc replaces magnesium. The octahedral coordination of zinc at the normal magnesium-binding site in chain *C* is shown. Zinc is shown in dark orange and the coordinated water molecules in light blue. The dashed red lines indicate the zinc-coordination interactions. The $F_o - F_c$ map is shown in gray at 20σ and was calculated without zinc. (*c*) Coordination of zinc by switch II. Each residue participating in the coordination of zinc (dark orange) is drawn in both chain *A* (magenta) and a symmetry-related chain *A* (green). The coordination of zinc is indicated by dashed red lines. The $F_o - F_c$ map is drawn in gray at a contour level of 20σ and was calculated without the Zn atom. The asterisk indicates a residue donated from a Rac1 in a crystallographically related asymmetric unit. (*d*) Crystal-packing interaction involving zinc. Residues from chain *A* are shown in magenta and residues from a symmetry-related chain *C* are shown in green. The coordination of zinc is indicated by dashed red lines. The $F_o - F_c$ map is drawn in gray at a contour level of 9σ and was calculated without the Zn atom. The asterisk indicates a residue donated from a Rac1 in a crystallographically related asymmetric unit.

3.2. Zinc coordination by Rac1

In the original molecular-replacement structure to 2.2 Å, four zinc sites were placed owing to the crystallization conditions and by homology to known zinc-coordinating protein structures. To verify these assignments experimentally, another data set was obtained at the zinc absorption edge in order to find the heavy-atom sites using the anomalous

differences. As shown in Fig. 2 and Table 1, the anomalous signal in the data set revealed that the crystal in fact contained eight zinc sites. Four of the zinc sites were those previously assigned (Figs. 3*a* and 3*c*), but the data also revealed four additional anomalous scatterers (Figs. 3*b* and 3*d*). Although Rac1 has not previously been shown to bind zinc, it is clear that there are Zn atoms present in the crystal structure based on the crystallization conditions, the anomalous data, the calculated electron-density maps and comparison with known crystal structures containing zinc. As stated in §2, high concentrations of $ZnSO_4$ were used in the crystallization conditions and could not be removed or replaced with other salts such as $MgSO_4$. Additionally, the $F_o - F_c$ density is drawn as gray wire in Fig. 3 for each assigned site, showing the clear presence of a large difference density. The $F_o - F_c$ map was generated without the Zn atom and is drawn in gray at a contour level of 20σ for Figs. 3(*a*)–3(*c*) and at 9σ for Fig. 3(*d*). The modeling of zinc in the Rac1 structure caused an overall fall in R_{work} and R_{free} of 3.1% and 3.5%, respectively. Similar effects on the refined R values have been observed previously for macromolecular structures containing zinc (Papageorgiou *et al.*, 1995)

As expected and as demonstrated by our data, most of the zinc sites are tetrahedrally coordinated, which is the most common mode of zinc coordination in proteins (Alberts *et al.*, 1998; Dudev & Lim, 2003). The central zinc (Figs. 2 and 3*a*) is coordinated by the carboxyl group of an aspartic acid residue from each monomer (Asp38) and the coordination is completed by a water molecule to generate a tetrahedral geometry. In Figs. 3(*c*) and 3(*d*) a similar configuration is observed, with all donating atoms belonging to side-chain residues. In contrast, Fig. 3(*b*) shows that zinc is coordinated in an octahedral geometry by Thr35, Thr17, GDP and three water molecules. This was in contrast to the original model, in which magnesium was assigned to this site. Normally, Rac1 uses magnesium to coordinate and bind GDP and this coordination contributes significantly to the binding energy of the nucleotide and overall stability (Vetter & Wittinghofer, 2001; Hakoshima *et al.*, 2003). Based on these considerations, it was at first surprising to see magnesium displaced but the GDP molecule still binding tightly. Although initially unexpected, zinc is known to adopt an octahedral coordination and, more importantly, zinc has been shown to displace magnesium in both protein and RNA structures, as the two atoms have similar coordination properties and ionic radii (Dudev & Lim, 2001, 2003; Ennifar *et al.*, 2001). Additionally, the work of Dudev and coworkers clearly demonstrated that zinc has a higher affinity than magnesium for the octahedral coordination sites that magnesium adopts in protein structures (Dudev & Lim, 2001). Owing to the high concentration of zinc in the crystallization buffer (§2) and the contribution of the Rac1 P-loop to nucleotide binding (Hutchinson & Eccleston, 2000), zinc, which is normally hexahydrated in solution, is most likely to have replaced magnesium before the GDP could be released. Moreover, these zinc sites represented the largest peaks in the anomalous signal. This, in conjunction with our data, demonstrates that zinc can fill the role of magnesium in GDP coordination of Rac1 molecules.

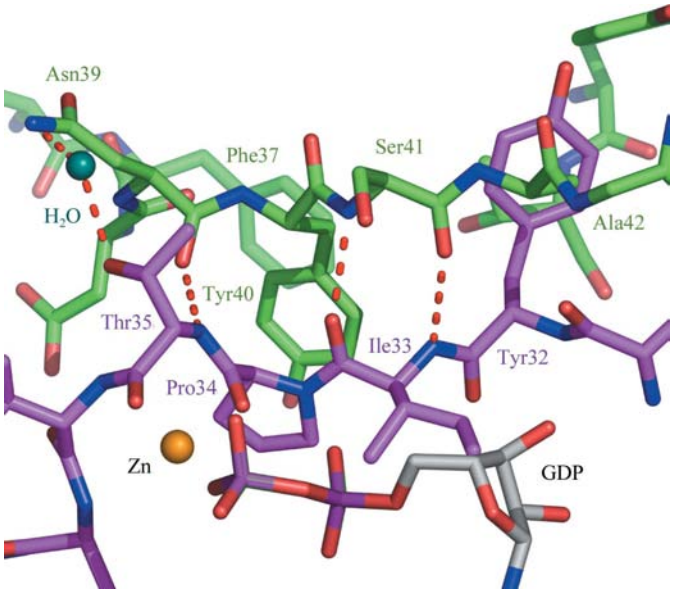

Figure 4
The intermolecular interactions at switch I as viewed between chain *A* (violet) and chain *C* (green). All residues from chain *A* are labeled in violet and all residues from chain *C* are labeled in green. Water molecules are labeled in dark green and Zn atoms in orange. All non-C atoms in the protein chains are colored with red indicating oxygen and blue indicating nitrogen. Hydrogen-bonding interactions are indicated by dotted red lines.

3.3. Intermolecular interactions at switch I stabilize the Rac1 trimer

Rac1 bound to GDP behaves as a monomer in solution as assayed by gel filtration (Stebbins & Galan, 2000; Prehna *et al.*, 2006), making the Rac1–GDP–Zn complex crystal structure unexpected. Although there are several packing interactions that stabilize the crystal, the asymmetric unit has extensive intermolecular interactions that promote the trimer structure. Most of the intersubunit contacts within the asymmetric unit are isolated to switch I and occur at residues 31–35, 39–42 and 37 (Fig. 4). As described in Fig. 4, at each apex of the triangle-like structure formed by switch I owing to the tetrahedral coordination of zinc (Fig. 2) the switch region from each Rac1 monomer forms an intermolecular β-sheet with the subsequent monomer in the trimer. This is a continuation of the β-sheet formed between β-sheets 1, 2 and 3 in each Rac1 monomer. Overall, the intersubunit interactions provide a contact area of approximately 900 Å^2 between each monomer to give a total of 2699 Å^2. An example of this interaction is shown in Fig. 4 with chain *A* in violet and chain *C* in green. Main-chain hydrogen bonds are formed between the N atom of Ile33 of chain *A* and the carbonyl O atom of Ser41 in chain *C*, the carbonyl O atom of Ile33 in chain *A* and the N atom of Ser41 in chain *C*, the N atom of Thr35 in chain *A* and the carbonyl O atom of Asn39 in chain *C*. One side-chain polar interaction stabilizes this interface and consists of a water-mediated hydrogen bond that is formed between the hydroxyl

of Thr35 in chain *A*, a water molecule and the N atom of the carbonyl group of Asn39 in chain *C*. Additionally, other residues near switch I complete the binding surface. Tyr32 from chain *A* makes several main-chain and side-chain van der Waals interactions with the chain *A* residues Tyr23, Ala42 and Leu55. Residue Phe37 of chain *C* makes intramolecular van der Waals contacts with Tyr40 to position it to make a hydrophobic contact with the main-chain atoms of Ile33 and the side chain of Pro34, both from chain *A*.

In addition to the protein–protein interactions that stabilize the Rac1 trimer, the trimer itself seems to be formed and stabilized by the coordination of a Zn atom by the switch I regions of each of the Rac1 monomers (Fig. 3*a*). Specifically, as illustrated in Fig. 3(*a*) and described previously, Asp38 is involved in the tetrahedral coordination of a Zn atom. It seems apparent from this configuration that the resulting Rac1 trimer is a result of the tetrahedral coordination of the Zn atom by the switch I regions of each monomer.

3.4. The coordination of zinc stabilizes the Rac1–GDP–Zn crystal structure

The Rac1–GDP–Zn complex crystal is stabilized by symmetry-related packing interactions at three surfaces, two of which involve zinc coordination. One crystallographic contact does not contain zinc, but involves interactions at the C-terminal helix and consists of residues 117, 121, 127, 131, 138–140, 156, 163, 167 and 170 of each Rac1 molecule. These surfaces mainly constitute a hydrophobic van der Waals packing surface with the same residues in a symmetry-related molecule of Rac1. In contrast, the other two intermolecular interactions are primarily mediated through zinc coordination. The first is shown in Fig. 3(*d*) and involves the tetrahedral coordination of zinc. Two glutamic acid residues (Glu127 and Glu131) from each symmetry-related chain *A* and *C* form a tight interaction stabilizing crystal formation by zinc binding. The second site is more extensive, involving zinc coordiation at switch II and several van der Waals and polar interactions (Fig. 5). At the surface, each Rac1 monomer forms the same bonding interactions with a related Rac1 molecule across a twofold crystallographic symmetry axis. For simplicity, the interaction between chain *A* and another chain *A* from a symmetry-related asymmetric unit is used as an example (Fig. 5).

The contact surface including switch II is at a crystallographic twofold axis of symmetry and is primarily polar in nature (Fig. 5). Each tyrosine residue 64 forms a water-mediated hydrogen bond with the main chain of residue His104 from a symmetry-related Rac1 molecule. Specifically, the hydroxyl group of Tyr64 in one chain contacts a water molecule which is hydrogen bonded to the main-chain carbonyl O atom of His104 from the related chain. Arg68 of each monomer makes a hydrogen bond from its side chain to the main-chain carbonyl O atom of the symmetry-related Asp63, and Glu62 of chain *A* is part of a hydrogen-bond network with the imidazole ring of His104, a water molecule and the hydroxyl group of Ser71 (not shown). This network is completely within the same protein chain, apart from the solvent interactions, and seems to help position His104 for its role in zinc coordination (Figs. 3*c* and 5).

The core interactions of this surface are residues Asp63, Glu100, His104 and His103 from the symmetry-related Rac1 molecule, which coordinate a Zn atom (Figs. 3*c* and 5*a*). This intermolecular interaction has two coordinated Zn atoms;

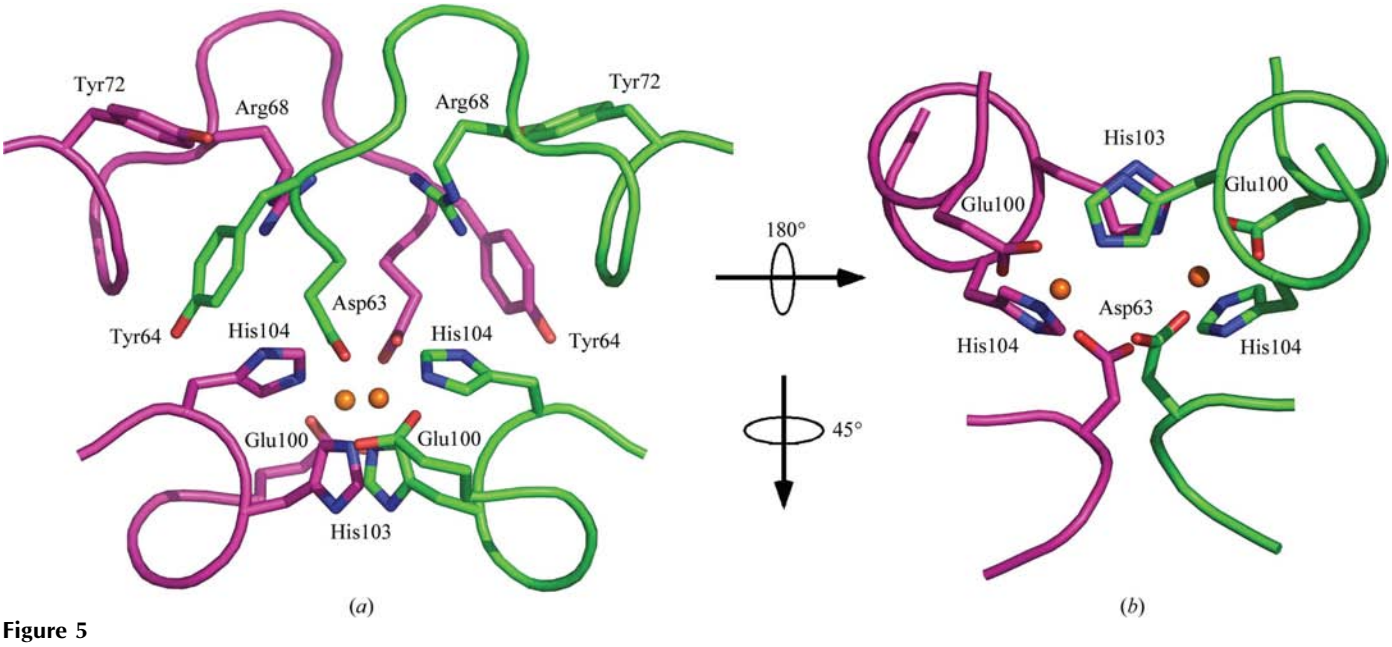

Figure 5
Zinc-coordination site at a twofold crystallographic axis of symmetry. (*a*) Chain *A* (magenta) and a symmetry-related chain *A* (green) and their intermolecular contacts are shown. Zinc is colored dark orange and all amino acids are labeled in black. (*b*) A view of the residues at the interface that are involved in zinc coordination after a 180° and 45° rotation as described in the figure. Chain *A* is colored magenta and a symmetry-related chain *A* is colored green.

each monomer donates residue His103 as a zinc-coordinated residue in a 'swapping' interaction with its symmetry-related element. Each His103 residue is further stabilized by van der Waals stacking with the symmetry-related His103 residue. This coordination is also tetrahedral and is reminiscent of the zinc coordination seen in the SEC2 crystal structure (Papageorgiou *et al.*, 1995). In this structure, zinc was coordinated by two acidic residues and two histidines, with one residue being donated from a crystallographically related molecule. In these studies, zinc was also reported to be needed for efficient crystallization of SEC2.

3.5. Zinc-induced conformations of switch I and switch II

The conformation of switch I when compared with known structures shows that it adopts the canonical GDP-bound conformation as expected (Fig. 6). Switch I is almost identical in conformation to the YpkA–Rac1–GDP complex and thus identical to the conformation seen in RhoGDI–Rac1–GDP complexes and RhoA–GDP (Wei *et al.*, 1997; Prehna *et al.*, 2006). What is even more striking is that the zinc-coordinated Rac1 trimer allows Thr35 to be stabilized by a hydrogen-bonding interaction with a water molecule and Asn39 of switch I in a subsequent Rac1 monomer (Fig. 4). Thr35 of Rac1 is important in magnesium binding, and thus GDP binding, and molecules such as GDIs specifically stabilize this residue with a hydrogen-bonding interaction to prevent nucleotide dissociation (Scheffzek *et al.*, 2000; Grizot *et al.*, 2001). It seems possible from this analysis that the oligomerization induced by zinc stabilizes the switch I region in the GDP-bound state and would prevent GDP dissociation.

As previously described in Fig. 5, switch II is also involved in zinc coordination and undergoes a drastic conformational change upon binding zinc. Normally, switch II adopts one of two discrete canonical conformations based on its bound nucleotide (Fig. 6). In contrast, switch II in the Rac1–GDP–Zn complex structure seems to adopt a completely novel fold based on zinc coordination. The coordination of zinc alters the fold of switch II, rearranging the hydrophobic packing interactions and significantly displacing key elements of switch I. Normally, Tyr72 participates in the hydrophobic core at switch II but, as shown in Fig. 5, it rotates out to face a symmetry-related Rac1 molecule to make packing interactions. Its role in stabilizing the hydrophobic core is filled by Leu70, which moves into almost the same position that Tyr72 fills in other Rac1 structures. Residue Gln61, which is involved in the intrinsic GTPase activity of Rac1, is moved ∼7.4 Å and residues Glu62 and Asp63, the latter of which is involved directly in zinc coordination, are both moved ∼10 Å from their position compared with the GDP-bound conformation of Rac1.

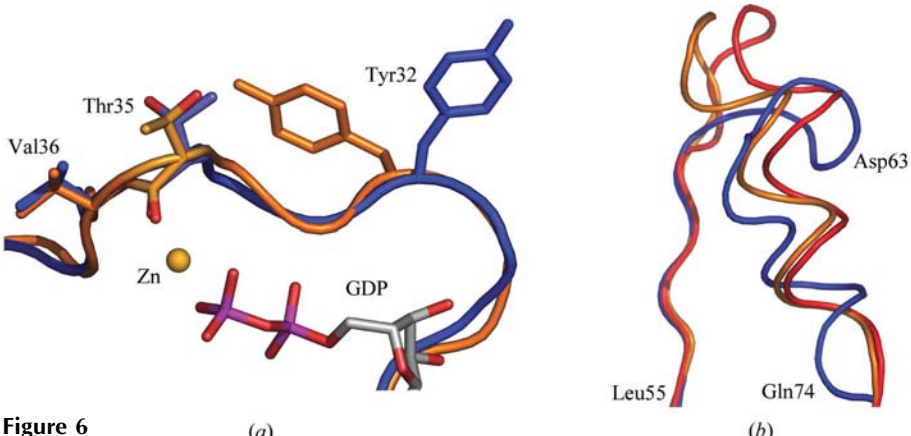

Figure 6
The conformations of switch I and switch II. (*a*) The conformation of switch I is the canonical GDP-bound form. Switch I from the Rac1–GDP–zinc complex is shown in blue and aligned with a YpkA–Rac1–GDP complex (shown in orange). The zinc ion and the GDP shown are from the Rac1–GDP–zinc complex. (*b*) Switch II adopts a novel conformation. Switch II (blue) was aligned with a YpkA–Rac1–GDP complex (orange) and the RhoGDI-2–Rac2 complex (red). The approximate locations of residues in the switch II structure of the Rac1–GDP–zinc complex are labeled in black.

4. Conclusions

Here, we present the structure of a Rac1–GDP–Zn complex at 1.9 Å resolution, which reveals the surprising ability of Rac1 molecules to form a trimer owing to the coordination of zinc. Moreover, zinc-coordination sites at packing surfaces stabilize the crystal structure and zinc coordination influences the conformation of the biologically important switch regions. Additionally, although magnesium is known to form an octahedral coordination site at switch I to facilitate the binding of GDP, our data suggest that zinc can replace the role of magnesium in GDP binding.

Zinc is found in a large number of crystal structures and can serve a myriad of biological purposes (Alberts *et al.*, 1998). The coordination of zinc by biological structures has been shown to be important in catalysis, such as in the protease thermolysin and the alcohol dehydrogenase htADH (Holden & Matthews, 1988; Ceccarelli *et al.*, 2004), structural stabilization, also in alcohol dehydrogenases and in the tumor suppressor p53 (Meplan *et al.*, 2000; Ceccarelli *et al.*, 2004), and for macromolecular binding, such as in zinc fingers (Brown, 2005). However, other crystal structures are known where zinc is simply present in the crystal and has no biological function. An example is the zinc-containing structure of the protease tonin, which has a zinc-coordination site similar to that of SEC2 (Papageorgiou *et al.*, 1995). In this structure, the protein was crystallized in zinc-containing buffer and it was concluded that zinc had no biological role within the context of the protease (Fujinaga & James, 1987).

Despite the observation that zinc is present in our crystal structure and that zinc can replace the role of magnesium in GDP binding, one must consider that the cytosolic concentration of zinc relative to magnesium is extremely low, with femtomolar ranges for zinc compared with millimolar ranges for

magnesium (Outten & O'Halloran, 2001; Dudev & Lim, 2003). In the cell, the concentration of zinc is kept far below that of magnesium owing to the sequestering of zinc into specialized compartments (Dudev & Lim, 2001; Eide, 2006). Eukaryotic cells have devoted several genes to the regulation of zinc concentration within various cellular compartments; free zinc is stored in 'zincosomes' and zinc concentration has been related to apoptosis (Truong-Tran *et al.*, 2000; Eide, 2006). Such considerations argue that it is unlikely that zinc binding would play a role in the regulation of RhoGTPase function *in vivo* and that the novel conformations induced by zinc binding are not likely to be present in the normal physiological state of the cell. Therefore, despite the intriguing possibilities raised for the regulation of RhoGTPase function by zinc, without further biological mandate our results remain at present tied tightly to the artificial environment of the crystallization conditions.

We thank Nikola Pavletich at Sloan Kettering for use of his X-ray facility and Babu A. Manjasetty of Brookhaven beamline X3A for access to and assistance with crystallographic equipment. This work was funded in part by research funds to CES from the Rockefeller University and PHS grants 1U19AI056510 (to CES).

References

Aktories, K. & Barbieri, J. T. (2005). *Nature Rev. Microbiol.* **3**, 397–410.
Alberts, I. L., Nadassy, K. & Wodak, S. J. (1998). *Protein Sci.* **7**, 1700–1716.
Bishop, A. L. & Hall, A. (2000). *Biochem. J.* **348**, 241–255.
Brown, R. S. (2005). *Curr. Opin. Struct. Biol.* **15**, 94–98.
Brünger, A. T., Adams, P. D., Clore, G. M., DeLano, W. L., Gros, P., Grosse-Kunstleve, R. W., Jiang, J.-S., Kuszewski, J., Nilges, M., Pannu, N. S., Read, R. J., Rice, L. M., Simonson, T. & Warren, G. L. (1998). (1998). *Acta Cryst.* D**54**, 905–921.
Ceccarelli, C., Liang, Z. X., Strickler, M., Prehna, G., Goldstein, B. M., Klinman, J. P. & Bahnson, B. J. (2004). *Biochemistry*, **43**, 5266–5277.
Collaborative Computational Project, Number 4 (1994). *Acta Cryst.* D**50**, 760–763.
DeLano, W. L. (2002). *The PyMOL Molecular Graphics System.* DeLano Scientific, San Carlos, CA, USA.
Dudev, T. & Lim, C. (2001). *J. Phys. Chem. B*, **105**, 4446–4452.
Dudev, T. & Lim, C. (2003). *Chem. Rev.* **103**, 773–788.
Dvorsky, R. & Ahmadian, M. R. (2004). *EMBO Rep.* **5**, 1130–1136.
Eide, D. J. (2006). *Biochim. Biophys. Acta*, **1763**, 711–722.
Ennifar, E., Walter, P. & Dumas, P. (2001). *Acta Cryst.* D**57**, 330–332.
Fujinaga, M. & James, M. N. (1987). *J. Mol. Biol.* **195**, 373–396.
Grizot, S., Faure, J., Fieschi, F., Vignais, P. V., Dagher, M.-C. & Pebay-Peyroula, E. (2001). *Biochemistry*, **40**, 10007–10013.
Hakoshima, T., Shimizu, T. & Maesaki, R. (2003). *J. Biochem. (Tokyo)*, **134**, 327–331.
Hirshberg, M., Stockley, R. W., Dodson, G. & Webb, M. R. (1997). *Nature Struct. Biol.* **4**, 147–152.
Holden, H. M. & Matthews, B. W. (1988). *J. Biol. Chem.* **263**, 3256–3260.
Hutchinson, J. P. & Eccleston, J. F. (2000). *Biochemistry*, **39**, 11348–11359.
Jaffe, A. B. & Hall, A. (2005). *Annu. Rev. Cell Dev. Biol.* **21**, 247–269.
Maesaki, R., Ihara, K., Shimizu, T., Kuroda, S., Kaibuchi, K. & Hakoshima, T. (1999). *Mol. Cell*, **4**, 793–803.
Meplan, C., Richard, M. J. & Hainaut, P. (2000). *Oncogene*, **19**, 5227–5236.
Murshudov, G. N., Vagin, A. A. & Dodson, E. J. (1997). *Acta Cryst.* D**53**, 240–255.
Otwinowski, Z. & Minor, W. (1997). *Methods Enzymol.* **276**, 307–326.
Outten, C. E. & O'Halloran, T. V. (2001). *Science*, **292**, 2488–2492.
Papageorgiou, A. C., Acharya, K. R., Shapiro, R., Passalacqua, E. F., Brehm, R. D. & Tranter, H. S. (1995). *Structure*, **3**, 769–779.
Perrakis, A., Morris, R. & Lamzin, V. S. (1999). *Nature Struct. Biol.* **6**, 458–463.
Potterton, E., Briggs, P., Turkenburg, M. & Dodson, E. (2003). *Acta Cryst.* D**59**, 1131–1137.
Prehna, G., Ivanov, M. I., Bliska, J. B. & Stebbins, C. E. (2006). *Cell*, **126**, 869–880.
Scheffzek, K., Stephan, I., Jensen, O. N., Illenberger, D. & Gierschik, P. (2000). *Nature Struct. Biol.* **7**, 122–126.
Stebbins, C. E. & Galan, J. E. (2000). *Mol. Cell*, **6**, 1449–1460.
Symons, M. & Settleman, J. (2000). *Trends Cell Biol.* **10**, 415–419.
Terwilliger, T. (2004). *J. Synchrotron Rad.* **11**, 49–52.
Truong-Tran, A. Q., Ho, L. H., Chai, S. & Zalewski, P. D. (2000). *J. Nutr.* **130**, 5S *Suppl.*, 1459S–1466S.
Van Aelst, L. & D'Souza-Schorey, C. (1997). *Genes Dev.* **11**, 2295–2322.
Vetter, I. R. & Wittinghofer, A. (2001). *Science*, **294**, 1299–304.
Wei, Y., Zhang, Y., Derewenda, U., Liu, X., Minor, W., Nakamoto, R. K., Somlyo, A. V., Somlyo, A. P. & Derewenda, Z. S. (1997). *Nature Struct. Biol.* **4**, 699–703.